

## RESEARCH ARTICLE



# Structural insights into the unique recognition module between $\alpha$ -synuclein peptide and nanobody

Zeyaul Islam<sup>1</sup> | Nishant N. Vaikath<sup>2</sup> | Issam Hmila<sup>2</sup> | Omar M. A. El-Agnaf<sup>2</sup> | Prasanna R. Kolatkar<sup>1</sup>

<sup>1</sup>Diabetes Center, Qatar Biomedical Research Institute, Hamad Bin Khalifa University, Qatar Foundation, Doha, Qatar

<sup>2</sup>Neurological Disorder Research Center, Qatar Biomedical Research Institute, Hamad Bin Khalifa University, Qatar Foundation, Doha, Qatar

## Correspondence

Prasanna R. Kolatkar, Diabetes Center, Qatar Biomedical Research Institute, Hamad Bin Khalifa University, Qatar Foundation, Doha 34110, Qatar.  
Email: [pkolatkar@hbku.edu.qa](mailto:pkolatkar@hbku.edu.qa)

## Funding information

QBRI, Grant/Award Number: IGP3

**Review Editor:** Carol Beth Post

## Abstract

Nanobodies are single-domain fragments of antibodies with comparable specificity and affinity to antibodies. They are emerging as versatile tools in biology due to their relatively small size. Here, we report the crystal structure of a specific nanobody Nb $\alpha$ -syn01, bound to a 14 amino acid long peptide of  $\alpha$ -synuclein ( $\alpha$ Syn), a 140-residue protein whose aggregation is associated with Parkinson's disease. The complex structure exhibits a unique binding pattern where the  $\alpha$ Syn peptide replaces the N-terminal region of nanobody. Recognition is mediated principally by extended main chain interaction of the  $\alpha$ Syn peptide and specificity of the interaction lies in the central 48–52 region of  $\alpha$ Syn peptide. Structure-guided truncation of Nb $\alpha$ -syn01 shows tighter binding to  $\alpha$ Syn peptide and improved inhibition of  $\alpha$ -synuclein aggregation. The structure of the truncated complex was subsequently determined and was indistinguishable to full length complex as the full-length form had no visible electron density for the N-terminal end. These findings reveal the molecular basis for a previously unobserved binding mode for nanobody recognition of  $\alpha$ -synuclein, providing an explanation for the enhanced binding, and potential for an alternate framework for structure-based protein engineering of nanobodies to develop better diagnostic and therapeutic tools.

## KEYWORDS

amyloids, nanobody, nanobody-peptide complex, Parkinson's disease, peptide binding, structure determination, unique paratopes,  $\alpha$ -synuclein

## 1 | INTRODUCTION

Parkinson's disease (PD) is the second most common human progressive neurodegenerative disorder among the elderly and the clinical symptoms include muscular rigidity, tremor, postural instability, and cognitive

impairment (Clarke, 2007; Forno, 1996; Wirdefeldt et al., 2011). The major characteristic of PD is the presence of intracellular aggregates/inclusions, known as Lewy bodies, and Lewy neuritis in the dopaminergic neurons of the substantia nigra pars compacta and several other regions of the nervous system (Cookson, 2005;

This is an open access article under the terms of the [Creative Commons Attribution-NonCommercial-NoDerivs](https://creativecommons.org/licenses/by-nc-nd/4.0/) License, which permits use and distribution in any medium, provided the original work is properly cited, the use is non-commercial and no modifications or adaptations are made.

© 2023 The Authors. *Protein Science* published by Wiley Periodicals LLC on behalf of The Protein Society.

Davie, 2008; Forno, 1996). The major constituents of these aggregates are pre-synaptic protein  $\alpha$ -synuclein ( $\alpha$ -syn/ $\alpha$ Syn) that lead to neuronal loss (Baba et al., 1998; Chiti & Dobson, 2006; Cookson, 2005). Additionally, the aggregation of  $\alpha$ -syn has been associated with several other neurological disorders, including dementia with Lewy bodies and multiple system atrophy (MSA) (Dickson, 1999; Newell et al., 1999; Spillantini et al., 1998; Wakabayashi et al., 1998). Moreover, several mutations in the  $\alpha$ -syn gene have been identified with autosomal dominantly inherited early onset PD and dementia with Lewy bodies (Chartier-Harlin et al., 2004; Krüger et al., 1998; Polymeropoulos et al., 1997; Zarranz et al., 2004).

$\alpha$ -Syn is a 140 amino acids long, intrinsically disordered protein, containing three distinctive regions: a positively charged N-terminal (residues 1–60), central non-amyloid component (NAC, residues 61–95), and negatively charged C-terminal region (residues 96–140). Although the monomeric  $\alpha$ -syn is natively unfolded, it assumes conformations that are stabilized by long range interactions between the acidic C-terminal and the central NAC (Bertoncini et al., 2005). The mechanisms underlying the structural transition of  $\alpha$ -syn to neurotoxic fibrillar forms are well-studied and have a range of oligomeric species (Conway et al., 2001; Rochet et al., 2000; Volles & Lansbury, 2003). These oligomeric species assemble further to generate protofibrils that finally convert into mature amyloid fibrils. Each protofibril adopts a five-stranded  $\beta$ -sheet conformation, intertwined in the final fibrillar form. However, the first and last 30 residues (1–30 and 110–140) do not adopt a  $\beta$ -sheet conformation, and are consequently flexible and solvent accessible (Del Mar et al., 2005; Qin et al., 2007; Vilar et al., 2008).

Antibodies (Abs) are widely-employed tools in biomedical research and are used in diagnostics and as therapeutic agents due to their binding specificity and high affinity to target antigens. The diversity of binding specificity is created by sequence variation in two variable domains, the heavy chain (VH) and the light chain (VL) (Georgiou et al., 2014). Although the enormous sequence diversity creates the antigen specificity, some redundancy exists in combining the VH and VL (Mitchell & Colwell, 2018) domains. A more simpler system is provided by the class of heavy-chain antibodies found in camelids, known as nanobody (Nb). Nb is approximately 15 kDa variable heavy domain of heavy chain (VHH) domain, nearly 10 times smaller in size than a conventional Ab while retaining the comparable binding specificity (Muyldermans, 2013). They are homologous to the Ab VH domain, containing three highly variable loops (H1, H2, and H3), and in some cases can bind to Ab inaccessible epitopes (Nguyen et al., 2000;

Staus et al., 2016; Steyaert & Kobilka, 2011). Two (H1, H2) of the hypervariable loops in Nb are significantly shorter than the four hypervariable loop counterparts of bivalent Ab VH-VL domain complex that provide binding specificity. A comparable analysis of Nb-antigen and Ab-antigen complexes shows that the greatest structural variability is found in the Nb H3 loop particularly having long H3 loops (Li et al., 2016; Muyldermans, 2013; Nguyen et al., 2000; Sircar et al., 2011). Longer H3 loop of Nb acts like a finger-like protrusion and enables it to access the epitope cavities, generating the ability to bind tightly and specifically to antigens (Mitchell & Colwell, 2018). Several Nbs including PFFNB2, NbSyn2, and NbSyn87 have been reported that can specifically recognize  $\alpha$ -syn preformed and mature fibrils (Butler et al., 2016; Butler et al., 2022; Guillems et al., 2013). They recognize distinct epitopes of monomeric  $\alpha$ -syn and reduced the associated cellular toxicity (Iljina et al., 2017).

Here, we report an alternate mode for increasing the binding diversity of Nb by employing a unique mechanism. In our previous work, we obtained Nb $\alpha$ -syn01, after phage display selection of a single-domain antibody library originating from a camel immunized with  $\alpha$ -syn (Hmila et al., 2022). Epitope mapping revealed that the recognition lies in the N-terminal region of  $\alpha$ -syn (amino acid 42–56, 14 amino acid long). This nanobody was found to have higher affinity for  $\alpha$ -syn fibrils than monomeric form. We determined the Nb-complex structure at 1.25 Å, where the  $\alpha$ -syn peptide forms a  $\beta$ -strand at the N-terminal of Nb. Structurally guided truncation of Nb improves the binding affinity and specificity. Our work highlights the capacity for molecular specificity and recognition in Nb, suggesting the potential to engineer Nbs with higher affinity and specific binding for various diagnostics and therapeutic purposes.

## 2 | RESULTS AND DISCUSSION

### 2.1 | Structure of Nb $\alpha$ -syn01- $\alpha$ Syn peptide complex

We recently reported a nanobody, Nb $\alpha$ -syn01 against  $\alpha$ -syn that preferentially recognizes  $\alpha$ -syn fibrils compared to the monomeric form (Hmila et al., 2022). This Nb binds to the N-terminal region corresponding to residues 43–56 of  $\alpha$ -syn. To understand the structural basis of interaction between Nb $\alpha$ -syn01 and  $\alpha$ -syn, we determined the crystal structure of the complex between the full length Nb and core peptidic region (43–56 amino acids) of  $\alpha$ -syn. Nb $\alpha$ -syn01 was purified and incubated with the peptide before injecting the complex on gel filtration column. The eluted complex was subjected to concentration and crystallization. Similarly, purified

Nb $\alpha$ -syn01 without mixing with peptide was used for crystallization screening. Interestingly, only the complex yielded crystals which were used for diffraction and subsequent determination of the structure.

The crystal structure of Nb $\alpha$ -syn01- $\alpha$ -syn peptide complex was determined to a resolution of 1.25 Å by molecular replacement with one complex in the

asymmetric unit (Table 1). In the complex structure, we observe electron density only for the last 10 residues out of 14 of the peptide N-GVVHGVATVA-C corresponding to residues 47–56 of  $\alpha$ -syn, implying that the first four residues were highly flexible and are not likely involved in interaction with the Nb $\alpha$ -syn01. Nb $\alpha$ -syn01 adopts the typical immunoglobulin fold, which consists of nine

**TABLE 1** X-ray crystallography data collection, processing, and structure refinement statistics.

	Nb $\alpha$ -syn01- $\alpha$ Syn peptide	$\Delta$ NterNb $\alpha$ -syn01- $\alpha$ Syn peptide
<i>Data collection and processing</i>		
Wavelength (Å)	0.92	0.92
Resolution range (Å)	28.79–1.29	28.58–1.23
Last resolution shell (Å)	1.33–1.29	1.26–1.23
Space group	P22 <sub>1</sub> 2 <sub>1</sub>	P22 <sub>1</sub> 2 <sub>1</sub>
Cell parameters (Å)	$a = 30.44, b = 41.67, c = 85.56$	$a = 30.35, b = 41.62, c = 85.03$
Total no. of reflections	256,448	238,566
Unique reflections	28,726 (2790) <sup>a</sup>	31,814 (2048)
Overall $I/\sigma$ ( $I$ )	12.6 (5.5)	10.9 (1.2)
Completeness (%)	99.7 (99.0)	98.8 (89.4)
Multiplicity	8.9 (8.7)	7.5 (3.3)
CC (½)	0.98 (0.91)	0.99 (0.78)
$R_{\text{merge}}$ (%) <sup>b</sup>	13.1 (48.3)	8.3 (47.9)
Wilson B-factor (Å <sup>2</sup> )	17.17	14.98
<i>Refinement</i>		
Resolution range (Å)	28.79–1.29	28.58–1.23
$R_{\text{factor}}$ (%)	16.11	14.23
$R_{\text{free}}$ (%)	18.65	16.99
Number of atoms	1045	1105
Protein	948	952
Solvent	91	129
No. of protein residues	120	121
Ligand molecules	1 Glycerol	2 Glycerol
Average B factors (Å <sup>2</sup> )	23.51	22.06
Protein	21.57	18.81
Solvent	42.88	43.93
Root mean square deviation (RMSD)		
Bond lengths (Å)	0.005	0.006
Bond angles (°)	0.81	0.88
Ramachandran plot		
Most favored region (%)	98.28	98.29
Additionally allowed region (%)	1.72	1.71
Outliers (%)	0.00	0.00
Protein Data Bank code	8JLY	8JJV

<sup>a</sup>Values for the last resolution shell are in parentheses.

<sup>b</sup> $R_{\text{merge}} = \sum_{\text{hkl}} \sum_i |I_i(\text{hkl}) - \langle I(\text{hkl}) \rangle| / \sum_{\text{hkl}} \sum_i I_i(\text{hkl})$ , where  $I(\text{hkl})$  is the intensity of reflection hkl.

$\beta$ -strands, grouped into two  $\beta$ -sheets exposing three antigen-binding CDR loops (CDR-H1, CDR-H2, and CDR-H3) (Figure 1 and Figure S1a). The two  $\beta$ -sheets are connected by loops and stabilized by a highly conserved disulfide bond between residues C22 and C95. Noticeably, the Nb $\alpha$ -syn01 structure exhibits an especially long CDR-H3, which contains 14 amino acids and is stabilized by an additional disulfide bond formed between C106 (located in the CDR3) and C45 (located in the framework region 2 [FR2]) (Figure S1b). The C45–C106 disulfide bond not only stabilizes the long CDR-H3 region, but also divides it into two parts, an N-terminal part consisting of S97 to G105 and a short C-terminal part consisting of G107 to G110 (Figure S1b). The CDR-H3 of Nb $\alpha$ -syn01 extends outside of the nanobody core and provides a large surface area for the  $\alpha$ -syn peptide binding (Figure 1). The initial eight residues from N-terminal of

Nb $\alpha$ -syn01 were not modeled due to lack of electron density, highlighting the possibility of this section being unstructured. The  $\alpha$ -syn peptide occupies the position where the unbound Nb $\alpha$ -syn01 N-terminal residues usually lie in conventional nanobodies and thus the peptide is integrated into the Nb $\alpha$ -syn01 structure, forming a partial strand in a  $\beta$ -sheet (Figure 1).

The  $\alpha$ -syn peptide binds to Nb $\alpha$ -syn01 in an elongated conformation, inserting into a groove between the CDR-H3 and the FR1 of Nb $\alpha$ -syn01 (Figures 2a and S2).  $\alpha$ -Syn peptide binds the Nb $\alpha$ -syn01 through a large number of backbone hydrogen bonds that anchor the peptide near the N-terminal of Nb $\alpha$ -syn01 (Figure 2b). Notably, neither CDR-H1 nor CDR-H2 is directly involved in the interaction. The C-terminal residues, V52 to V55 of  $\alpha$ -Syn peptide form a  $\beta$ -strand that binds to the  $\beta$ -strand of FR1 of Nb $\alpha$ -syn01 in an antiparallel fashion through main

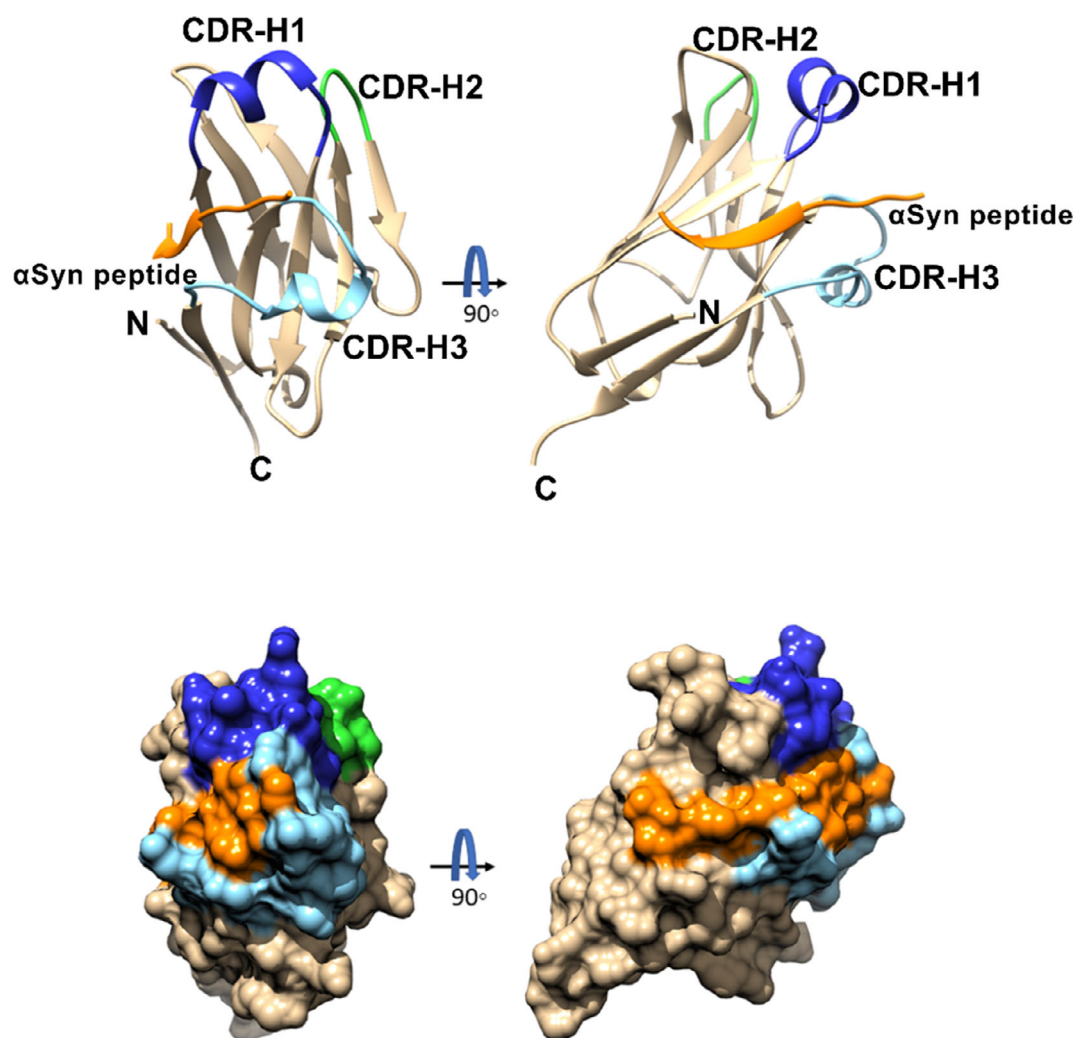


**FIGURE 1** Structure of  $\alpha$ -synuclein peptide bound Nb $\alpha$ -syn01. Overall structure of two perpendicular views of Nb $\alpha$ -syn01- $\alpha$ Syn peptide complex structure. Cartoon (upper panel) as well as surface (lower panel) representation highlighting the typical arrangement of the immunoglobulin fold of Nb $\alpha$ -syn01. Nanobody is shown as tan, indicating the three CDR loops CDR-H1, CDR-H2, and CDR-H3 as blue, green, and sky blue respectively. The  $\alpha$ Syn peptide is shown as orange.



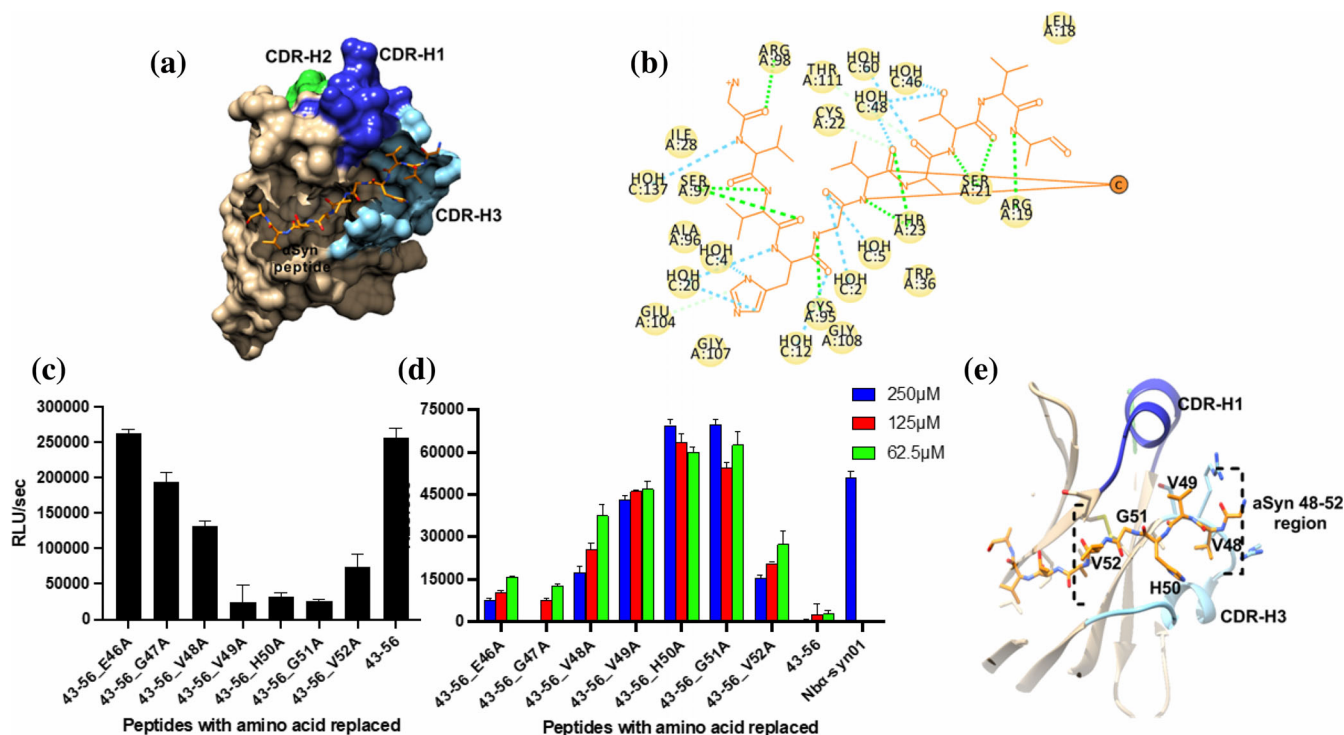


**FIGURE 2** Nbα-syn01-αSyn peptide binding pocket and epitope mapping of Nbα-syn01 using alanine scanning by ELISA. (a) Overall structure of the binding pocket with αSyn peptide (orange) shown as stick and Nbα-syn01 shown in surface representation. The CDR-H1 (blue) and CDR-H2 (green) are not directly participating in binding. (b) 2D diagram showing the interaction between Nbα-syn01 and αSyn peptide. The green dotted line represents the conventional hydrogen bonds and the light blue dotted line represents water mediated hydrogen bonds. (c) The chemiluminescence measurement of Nbα-syn01 binding to αSyn peptides. (d) Pre-incubating the peptides (62.5, 125, and 250 μM) with Nbα-syn01 followed by adding the complex to ELISA plate coated with α-syn. Nbα-syn01 showed a strong signal with peptide corresponding to amino acid 43–56 of α-syn. (e) Complex structure (Nbα-syn01-αSyn peptide) highlighting the central role of V48–V52 region of αSyn peptide.

chain interaction (Figure 2b). The CDR-H3, apart from using the main chain interaction, employs a R98 side chain to interact with the backbone carbonyl group in G47 of αSyn peptide (Figure 2b). Similarly, the side chain of S21 (Nbα-syn01) interacts with the side chain of T54 (αSyn peptide) through a water mediated hydrogen bond (Figure 2b).

Our efforts to crystallize the Nbα-syn01 alone were unsuccessful. Nevertheless, we modeled the Nbα-syn01 using Swiss-model (Waterhouse et al., 2018) (Figure S3a). Nanobody Nb22 (PDBID: 5h1r) was chosen as a template (sequence identity = 71.8%) which we also used as a search model for molecular replacement for solving the Nbα-syn01-α-syn peptide complex structure. The overall structure of the Nbα-syn01 had a topology of immunoglobulin fold, rich in β-strands and was very similar to the Nbα-syn01-α-syn peptide complex structure with root mean square deviation (RMSD) of 0.82 Å for 86 Cα. However, the comparison analysis revealed two major differences between these two structures (Figure S3b). A major conformational change was observed in the CDR-H3 region, where the complex adopts a more open conformation compared to the apoform Nbα-syn01. The open

conformation in complex was induced by the α-syn peptide and helps it to accommodate the extended α-syn peptide conformation. The other major difference lies in the N-terminal region, which was missing from our complex structure. The N-terminal region of apoform Nbα-syn01 occupied the same position of α-syn peptide of complex structure, revealing that the N-terminal of nanobody was “seemingly” displaced by α-syn peptide. However in our structure the N-terminal of the apo form is likely disordered and thus there is no displacement of this region but rather access to a unique paratope is granted. Overall, the superimposition of these two structures suggests that the α-syn peptide replaces the N-terminal region of nanobody (using a conventional Nb template) with concurrent opening of the CDR-H3 region.

## 2.2 | Specificity determinants of Nbα-syn01: α-syn peptide interaction

Our initial epitope mapping reveals a 14-mer (43–56) αSyn peptidic region, which binds to Nbα-syn01, and was

further confirmed by our complex structure determination showing that  $\alpha$ -syn peptide binds by occupying the location where N-terminal region of Nb $\alpha$ -syn01 would sit in a conventional nanobody. In our crystal structure we did not find the electron density of residues 43–46 of  $\alpha$ -syn peptide, suggesting their flexibility and precluding any interaction with the Nb $\alpha$ -syn01. The remaining 10 residues of  $\alpha$ -syn peptide were well resolved and bound to several residues of CDR-H3 (Figure 2b). We next determined the specificity of individual residues contributing to the interaction. To map the specificity determinants, we designed a series of alanine mutants spanning the whole stretch of  $\alpha$ -syn peptide (Table S1). Alanine scanning was carried out by two methods: first by coating the peptides onto ELISA plate and probing with the Nb $\alpha$ -syn01 and second by pre-incubating the peptides with Nb $\alpha$ -syn01 followed by addition of the complex to ELISA plate coated with  $\alpha$ -syn. In the first approach, reduced signal was observed when residues 48–52 were replaced with alanine (Figure 2c). Similarly, in the preabsorption experiment, a high signal can be seen when residues 48–52 were replaced (Figure 2d). Both these methods clearly identified the region 48–52 of  $\alpha$ -syn peptide as the epitope recognized by the Nb $\alpha$ -syn01. The results corroborated well with our complex structure where the residues 48–52 (N-GVVHGVATVA-C) occupy the central region and are stabilized through several main chain interactions (Figure 2e). Interestingly, several mutations including H50Q and G51D were reported in this region in early onset PD cases (Fares et al., 2014; Rutherford et al., 2014; Zarranz et al., 2004).

### 2.3 | Creation of N-terminal truncated $\Delta$ NterNb $\alpha$ -syn01

In our Nb $\alpha$ -syn01- $\alpha$ -syn peptide complex structure, we did not observe the first 8 amino acids of Nb $\alpha$ -syn01; instead, the N-terminal position was occupied by  $\alpha$ -syn peptide suggesting that removal of the N-terminal portion of Nb could either have no effect on complex formation or strengthen the binding affinity with  $\alpha$ -syn peptide as it would be entropically favored. In addition, a more compact nanobody would be created associated with potentially better specificity and solubility. We truncated the first eight residues from the N-terminal of Nb $\alpha$ -syn01 ( $\Delta$ NterNb $\alpha$ -syn01) using site-directed mutagenesis to validate our prediction.

To investigate the perturbation in secondary structural content in truncated,  $\Delta$ NterNb $\alpha$ -syn01, Circular dichroism (CD) experiments at far-UV region were carried out. The far-UV CD spectra of  $\Delta$ NterNb $\alpha$ -syn01 were similar to Nb $\alpha$ -syn01, revealing that the truncated nanobody

folds well in absence of N-terminal region (Figure 3a). Both the nanobodies were rich in  $\beta$ -sheet structure and the spectra were similar to the proteins with an immunoglobulin fold (Dumoulin et al., 2002; Williams et al., 2013). We also generated a point mutation S21A (serine to alanine at position 21) in Nb $\alpha$ -syn01, guided by our Nb $\alpha$ -syn01- $\alpha$ -syn peptide complex structure, where apart from main chain interaction,  $\alpha$ -syn peptide binds to S21 through water mediated side chain interaction. NbS21A exhibits a similar fold relative to Nb $\alpha$ -syn01 and is rich in  $\beta$ -sheet structure. Secondary structure content as analyzed by software BeStSel suggested having 35%–38%  $\beta$ -sheet structure for these three nanobodies (Table S2). The CD spectra of  $\alpha$ -syn peptide also suggested that the secondary structure is dominated by  $\beta$ -sheets (Figure 3b), observed in similar structures of other amyloidogenic short peptides (Reynolds et al., 2017).

To examine whether secondary structure changes occur upon binding of the nanobodies to  $\alpha$ -syn, we analyzed CD spectra of nanobodies and  $\alpha$ -syn peptide individually, as well as that of  $\alpha$ -syn peptide with equimolar mixtures of each nanobody (Figure 3b–d). The CD spectra of the three complexes (Nb $\alpha$ -syn01: $\alpha$ -syn peptide,  $\Delta$ NterNb $\alpha$ -syn01: $\alpha$ -syn peptide, and NbS21A: $\alpha$ -syn peptide) is the sum of the spectra of individual components, indicating that there is no change in the secondary structure composition upon complex formation. Importantly, the CD analysis indicates that nanobodies bind to  $\alpha$ -syn peptide with a native  $\beta$ -strand and complex formation did not significantly alter this structure. This also validates the hypothesis that the peptide isn't displacing any bound N-terminal Nb strands but is binding to a vacant paratope.

Isothermal titration calorimetry (ITC) was employed to measure the strength of nanobodies:  $\alpha$ -syn peptide interactions as well as to derive the associated thermodynamic parameters. Analysis of the ITC data reveals a 1:1 interaction for the Nbs with  $\alpha$ -syn peptide and dissociation constants (Kd) at 25°C of  $809 \pm 8.4$  and  $76 \pm 22.7$  nM, for Nb $\alpha$ -syn01 and  $\Delta$ NterNb $\alpha$ -syn01, respectively (Figure 4). The truncated nanobody binds to  $\alpha$ -syn peptide with 10.6-fold higher affinity than the wild type nanobody. The ITC measurements also indicate that both nanobody:  $\alpha$ -syn peptide interactions are predominantly enthalpically driven with the thermodynamic parameters values consistent with the range found for other antigen: antibody/nanobody interactions (Brockhaus et al., 2007; Williams et al., 2013). The comparative Kd and enthalpic values of the two nanobody:  $\alpha$ -syn peptide complexes suggests that  $\Delta$ NterNb $\alpha$ -syn01 has tighter interaction with the  $\alpha$ -syn peptide, due to more favorable enthalpic and entropic values resulting from the removal of N-terminal region.

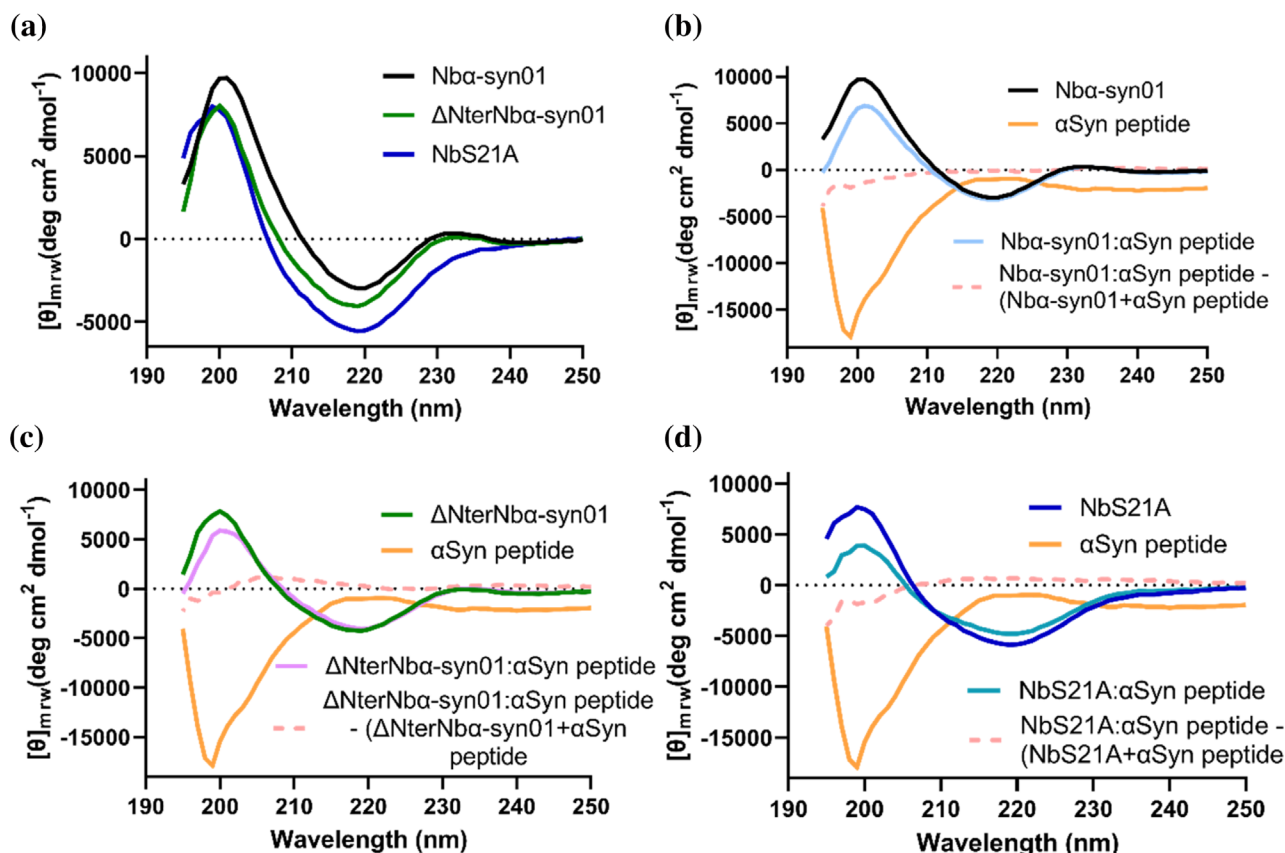


**FIGURE 3** Circular dichroism (CD) measurements of nanobodies and their interactions. (a) Far-UV CD spectra of Nb $\alpha$ -syn01 (black),  $\Delta$ NterNb $\alpha$ -syn01 (green) and NbS21A (blue). The spectra were measured at 25°C. The concentration of proteins were 10  $\mu$ M and the cell path lengths of 1 mm were used for far-UV (from 195 to 250 nm) data acquisition. (b) Nb $\alpha$ -syn01:  $\alpha$ Syn peptide interaction. The difference spectrum (complex) – (Nb $\alpha$ -syn01 +  $\alpha$ Syn peptide) is shown as a broken line. (c) CD measurements of the  $\Delta$ NterNb $\alpha$ -syn01:  $\alpha$ Syn peptide interaction. (d) CD measurements of the NbS21A:  $\alpha$ Syn peptide interaction. The  $\alpha$ Syn peptide is shown as orange traces in each panel. The difference spectrum is shown as a dotted line.

## 2.4 | Structure of $\Delta$ NterNb $\alpha$ -syn01- $\alpha$ Syn peptide complex

The crystal structure of  $\Delta$ NterNb $\alpha$ -syn01- $\alpha$ -syn peptide complex was determined to a resolution of 1.23 Å with one molecule of the complex in the asymmetric unit. It has a similar topology to the Nb $\alpha$ -syn01- $\alpha$ -syn peptide complex structure (Figure 5a). The superimposed structures of  $\Delta$ NterNb $\alpha$ -syn01- $\alpha$ -syn and Nb $\alpha$ -syn01- $\alpha$ -syn differ by a RMSD of 0.12 Å on all 111 aligned residues (Figure 5a). In fact structurally they are indistinguishable, highlighting that the removal of N-terminal region of Nb $\alpha$ -syn01 has no effect on the overall complex structure. One structure of nanobody bound to  $\alpha$ -syn peptide was previously known (de Genst et al., 2010), NbSyn2:  $\alpha$ -syn peptide (PDBID: 2 m  $\times$  6 m) corresponding to C-terminal residues 132–140 of  $\alpha$ -synuclein. The superposition of our complex structure with NbSyn2:  $\alpha$ -syn peptide shows RMSD of 0.76 Å for 90 C $\alpha$ , indicating that the overall fold of these structures remains similar

(Figure 5b). Despite having similar topology, the conformations of the Nb $\alpha$ -syn01 and NbSyn2 CDR-H3 region differ significantly (Figure 5b). More importantly, large differences observed in CDR3 region arise due to the fact that C-terminal  $\alpha$ -syn peptide binds NbSyn2 between the CDR-H2 and CDR-H3 (Figure 5b), which shifts the CDR-H3 towards CDR-H2. NbSyn2 binds specifically to monomeric  $\alpha$ -synuclein (de Genst et al., 2010) while our Nb $\alpha$ -syn01 prefers fibrils. The buried surface area analysis of our complex (interface area of 697.0 Å<sup>2</sup>) compared to NbSyn2:  $\alpha$ -syn peptide (interface area of 307.6 Å<sup>2</sup>) reveals the extensive buried surface area of our complex that leads to higher affinity. Nb $\alpha$ -syn01 explores the core fibrillar region of  $\alpha$ -syn by aligning its unique paratope having an unbound antiparallel  $\beta$ -stand (unlike 2 m  $\times$  6 m), explaining the preference of Nb $\alpha$ -syn01 for fibril. Conversely, NbSyn2 explores the unstructured region outside the core fibrillar region of  $\alpha$ -syn, aligning with the loops of CDRs, explaining its specificity towards monomeric form of  $\alpha$ -syn.

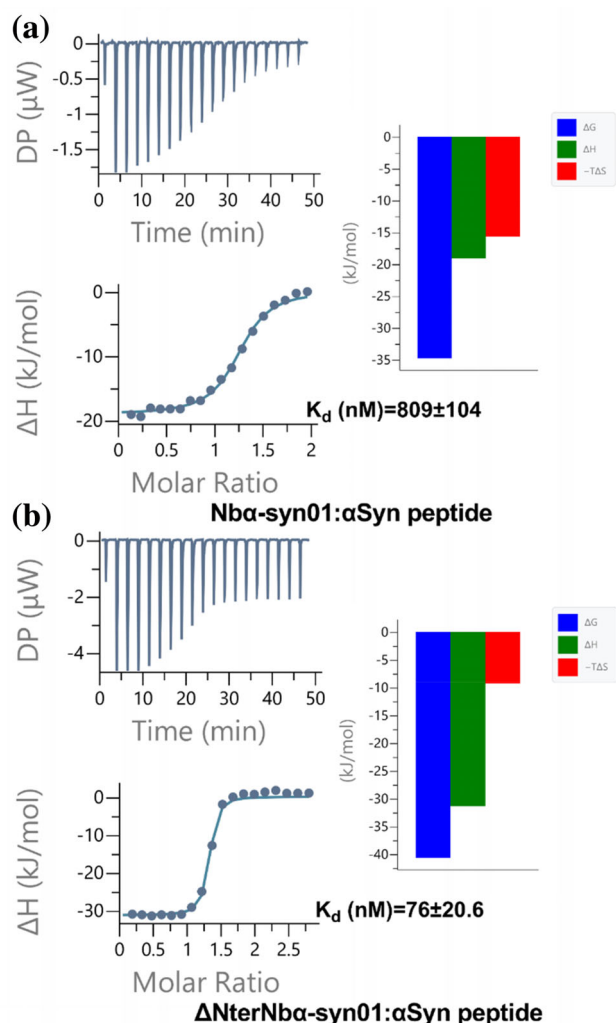


**FIGURE 4** Characterization of the interactions of Nbα-syn01 and ΔNterNbα-syn01 with αSyn peptide by isothermal titration calorimetry (ITC). (a) Titration of the αSyn peptide into Nbα-syn01. (b) Titration of the αSyn peptide into ΔNterNbα-syn01. ΔG, ΔH, and -TΔS were measured for the binding of Nbα-syn01/ΔNterNbα-syn01 with αSyn peptide and shown as signature plot. ΔNterNbα-syn01 binds more strongly to αSyn peptide than Nbα-syn01.

## 2.5 | Prevention of aggregation propensity of α-synuclein

We analyzed the in-vitro α-syn aggregation when using ΔNterNbα-syn01 and NbS21A in comparison to the Nbα-syn01. Our earlier results show that Nbα-syn01 inhibits α-syn-seeded aggregation in vitro and also reduced α-syn-seeded aggregation and toxicity in cells (Hmila et al., 2022). α-Syn seeds were incubated with these three nanobodies and after 1 h transferred in a tube containing α-syn monomers. The mixture was incubated up to 24 h and sampled at various time points. Nbα-syn01 and ΔNterNbα-syn01 were both found to

inhibit the in-vitro α-syn seeded aggregation (Figure 6). It was notable that the inhibition of aggregation was higher in ΔNterNbα-syn01 than Nbα-syn01, in agreement with expectations based on our complex structure (N-terminal region sampling fibrils) and ITC data (tighter binding). The NbS21A form did not inhibit the seeded aggregation as observed by initial Th-S signal; however, the aggregation was delayed compared to the control (Figure 6). The α-syn itself (without seeds) was shown not to aggregate under the conditions of these experiments.

## 3 | CONCLUSIONS

Our structural analysis of the Nbα-syn01-α-syn peptide complex revealed an unusual binding mode in which the α-syn peptide adopts a β-strand conformation and forms part of a β-sheet structure by complementing the open and exposed near N-terminal region of Nbα-syn01. The binding surface is formed by the N-terminal framework region and CDR-H3, which is conformationally open to accommodate the α-syn peptide. This is the first crystal structure of a nanobody that binds to peptide in such a manner, thus demonstrating a new way of creating the binding repertoire of nanobody. Numerous backbone hydrogen bonds provide high affinity, centered around the residues 48–52 of α-syn, as determined by epitope mapping using alanine scanning. Structure guided truncation (ΔNterNbα-syn01) and mutation NbS21A were designed and characterized in comparison to Nbα-syn01. We compared the folding status, secondary structure content, and perturbation in complex formation by CD. The findings suggest no change in secondary structure content in complex formation, indicating that the truncated N-terminal region was unstructured and α-syn peptide having β-strand occupies the N-terminal region in antiparallel fashion and forming a complementary β-sheet.

We show using ITC that the truncated version of Nbα-syn01 binds the α-syn peptide with approximately 10 fold higher affinity than Nbα-syn01 and the overall process is enthalpic driven but entropic contributions allow relative higher affinity of the truncated Nb. Determination of ΔNterNbα-syn01-α-syn peptide structure further confirms the rationale for stronger binding and also highlights that the truncation does not affect the complex formation. The designed truncated nanobody not only binds α-syn peptide tightly but also efficiently inhibits aggregation in vitro. These studies highlighted the potential of these nanobodies in diagnostic and therapeutic applications.



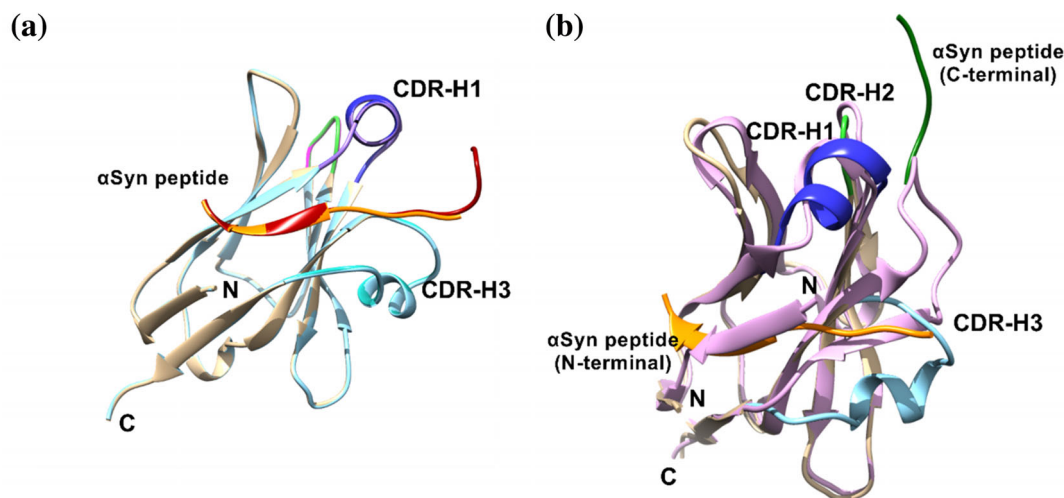


**FIGURE 5** Structure of  $\Delta$ NterNb $\alpha$ -syn01- $\alpha$ Syn peptide complex and structural comparisons: (a) Superposition of two complex structure, indicating their similarity in binding the  $\alpha$ Syn peptide. The  $\alpha$ Syn peptide is colored as dark red (in  $\Delta$ NterNb $\alpha$ -syn01 complex) and orange (in Nb $\alpha$ -syn01 complex). Three CDR-Hs in three different color. (b) Comparison of our structure (Nb $\alpha$ -syn01- $\alpha$ Syn peptide) with NbSyn2:  $\alpha$ Syn peptide (PDBID: 2 m  $\times$  6 m) corresponds to C-terminal residues 132–140 of  $\alpha$ -synuclein. Nbsyn2 is colored in light pink. The C-terminal  $\alpha$ Syn peptide is shown as dark green.

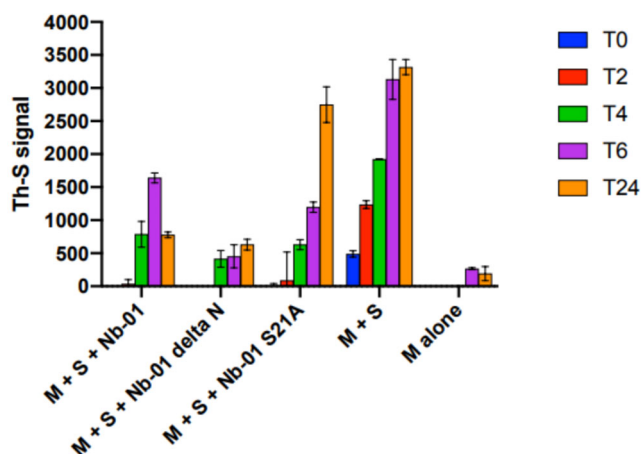


**FIGURE 6** In vitro aggregation assay. The aggregation  $\alpha$ -synuclein, monitored by Th-S binding assays at different time points (T0–T24) from the in-vitro seeding in presence of Nb $\alpha$ -syn01 (Nb-01),  $\Delta$ NterNb $\alpha$ -syn01 (Nb-01 delta N) and NbS21A (Nb-01 S21A).  $\alpha$ -Syn seeds (S) were incubated alone or in combination with Nb $\alpha$ -syn01,  $\Delta$ NterNb $\alpha$ -syn01 or NbS21A. The incubated samples were then added to tubes containing  $\alpha$ -syn monomers (M) in PBS. The fluorescence was sampled at various time points along the aggregation reaction.

## 4 | MATERIALS AND METHODS

### 4.1 | Generation and purification of nanobodies

Detailed protocols of immunization and construction of the nanobody phage library have been described previously (Hmila et al., 2022). In summary, a 3 year old

healthy male camel was weekly immunized 10 times, subcutaneously with  $\alpha$ -syn protein (1 mg/camel) emulsified in Freund's complete adjuvant followed by booster immunization in incomplete adjuvant.  $\alpha$ -Syn-specific nanobodies were selected by four consecutive rounds of in vitro phage display selection on a well plate coated with 10  $\mu$ g antigen per well. Specific phage particles were eluted with 100 mM triethylamine, (pH 10.0). The eluted particles were used to infect exponentially growing *Escherichia coli* TG1 cells. Enrichments of specific phage particles were assessed by comparing phage particle titers eluted from coated wells versus wells without antigen. After four rounds of panning, individual colonies were picked and identified by polyclonal phage ELISA. Positive clones were sequenced, and unique clones were transformed into *E. coli* WK6 competent cells. Nb $\alpha$ -syn01 was expressed in the periplasm of *E. coli* and purified using immobilized metal affinity chromatography and size exclusion chromatography according to published protocols (Hmila et al., 2022). The N-terminal truncated version of Nb $\alpha$ -syn01 (removal of first 8 amino acid residues),  $\Delta$ NterNb $\alpha$ -syn01, and the mutant S21A (NbS21A) were created by site directed mutagenesis using an overlap PCR extension method with suitable primers. The resultant plasmids were verified by sequencing and purified similarly as Nb $\alpha$ -syn01.

### 4.2 | Crystallization

Complexes were formed by incubating the Nb $\alpha$ -syn01 or  $\Delta$ NterNb $\alpha$ -syn01 with a threefold molar excess of  $\alpha$ Syn

peptide at 4°C for 1 h. The complexes were then purified by gel filtration chromatography using a Superdex 75 10/300 GL (GE Healthcare) using phosphate-buffered saline (PBS: 137 mM NaCl, 2.7 mM KCl, 10 mM Na<sub>2</sub>HPO<sub>4</sub>, 1.8 mM KH<sub>2</sub>PO<sub>4</sub>, pH 7.4) as running buffer. The Nb $\alpha$ -syn01- $\alpha$ Syn peptide complex was concentrated to 20 mg/mL and used for crystallization experiments using the sitting drop vapor diffusion method in a 96-well plate (MRC 2 well crystallization plates, Hampton Research, USA). Initial crystallization screens were performed with several commercial kits with each drop containing 0.2  $\mu$ L of protein mixed with 0.2  $\mu$ L of precipitant and equilibrated against 50  $\mu$ L of reservoir solution followed by incubation at 18°C. The crystallization conditions obtained from the initial screen were optimized in 15-well hanging drop crystallization plates (Qiagen, USA) at 18°C. Drops containing 2  $\mu$ L of protein and 2  $\mu$ L of reservoir solutions were equilibrated against 1 mL of reservoir solution. Nb $\alpha$ -syn01- $\alpha$ Syn peptide complex was crystallized in 0.1 M sodium acetate trihydrate pH 4.6, 2.0 M ammonium sulfate. Similarly,  $\Delta$ NterNb $\alpha$ -syn01- $\alpha$ Syn peptide complex was crystallized at 15 mg/mL in 0.1 M BIS-TRIS pH 5.5, 2.0 M ammonium sulfate.

### 4.3 | X-ray data collection and structure determination

Crystals were harvested into a solution of mother liquor with 25% (v/v) glycerol and flash-frozen in liquid nitrogen. Diffraction data for Nb $\alpha$ -syn01- $\alpha$ Syn peptide complex and  $\Delta$ NterNb $\alpha$ -syn01- $\alpha$ Syn peptide complex were obtained at the automated macromolecular crystallography (AMX)/17-ID-1 beamline of National Synchrotron Light Source II (NSLSII) located at Brookhaven National Laboratory (BNL) using 0.92 Å wavelength at 100 K. The diffraction images of all the data sets were indexed, integrated, and scaled using the XDS suite of programs (Kabsch, 2010). The Nb $\alpha$ -syn01- $\alpha$ Syn peptide complex crystal was diffracted to 1.25 Å while the  $\Delta$ NterNb $\alpha$ -syn01- $\alpha$ Syn peptide complex crystal was diffracted to 1.23 Å resolution (Table 1).

The Nb $\alpha$ -syn01- $\alpha$ Syn peptide complex structure was determined by molecular replacement using Phaser (McCoy et al., 2007) with one molecule of nanobody Nb22 (Protein Data Bank Code PDBID: 5lhr) as the search model. The initial model was refined as rigid body followed by restrained refinement using Refmac (Murshudov et al., 2011). The model was manually built using the program Coot (Emsley & Cowtan, 2004) after several rounds of refinement to improve the model. The model was further refined by iterative rounds of refinement in Phenix (Adams et al., 2010). The Nb $\alpha$ -

syn01- $\alpha$ Syn peptide complex model was employed as a search model for solving  $\Delta$ NterNb $\alpha$ -syn01- $\alpha$ Syn peptide complex structure by molecular replacement. The model was refined and built using Refmac, Coot, and Phenix. The Model quality assessment and Ramachandran plot statistics were calculated using Molprobit (Davis et al., 2007). All the structural analysis, figures with structural representations and superimposition were produced using the program UCSF Chimera (Pettersen et al., 2004).

### 4.4 | Circular dichroism measurements

The folding status and perturbation of the secondary structure was checked by CD. Samples of Nb $\alpha$ -syn01,  $\Delta$ NterNb $\alpha$ -syn01, and NbS21A were prepared at a concentration of 10  $\mu$ M in PBS buffer (pH 7.4). Similarly, sample containing only  $\alpha$ -syn peptide (10  $\mu$ M) and an equimolar mixture of  $\alpha$ -syn peptide (10  $\mu$ M) and each nanobody (10  $\mu$ M) were prepared. CD measurements were performed on a Chirascan CD spectrometer (Applied Photophysics) using a cuvette with a 0.1 cm path length. The temperature for the experiments was controlled with a Peltier temperature control unit (Quantum northwest). Spectra were recorded between 250 and 195 nm at 25°C. We collected five scans of each protein, averaged, and subtracted them from the buffer spectra. The acquired CD data were analyzed with the BeStSel (Beta Structure Selection) Server (<http://bestsel.elte.hu/index.php>) (Micsonai et al., 2018) to estimate the content of different secondary structures in the protein.

### 4.5 | Isothermal titration calorimetry studies

Calorimetric data of nanobody binding to  $\alpha$ -synuclein peptide were recorded using a MicroCal Auto-iTC200 microcalorimeter (Malvern, USA) at 25°C. We titrated 40  $\mu$ L solutions of  $\alpha$ -synuclein peptide, at a concentration of 400  $\mu$ M, in 2  $\mu$ L aliquots into the calorimetric cell containing a solution of Nb $\alpha$ -syn01 or  $\Delta$ NterNb $\alpha$ -syn01 (400  $\mu$ L of a 40  $\mu$ M). Total of 19 injections of the  $\alpha$ -syn peptide were mixed into the sample cell at 150 s intervals with stirring speed of 750 rpm. First initial small injection was used to minimize the impact of equilibration artifacts and was disregarded during evaluation of the data. As a control experiment, buffer solution was used in sample cell with same concentration of  $\alpha$ -syn peptide in syringe. Injections of the titrant into a cell that contained only buffer solutions were subtracted from the other binding experiments to correct for the heat

generated by dilution effects. The thermodynamic analysis was performed with the MicroCal PEAQ-ITC analysis software (Malvern instruments) by fitting the ITC isotherms with non-linear least squares regression method using a 1:1 bimolecular binding model.

#### 4.6 | Epitope mapping (alanine scanning)

To map the epitopes for Nb $\alpha$ -syn01, we performed alanine scanning, a widely used site-directed mutagenesis approach. Synthetic 14 amino acid long peptides spanning residues 43–56 (Table S1) of  $\alpha$ -syn were used based on the epitope mapped in previous study (Hmila et al., 2022). The exact epitope region was identified by two methods. In the first approach, a 384-well black MaxiSorb plate (Nunc) was coated with 500 ng/well of the peptides in NaHCO<sub>3</sub> and incubated overnight at 37°C under dry conditions. The following day, the plate was blocked with blocking buffer (PBST containing 2.25% gelatin) for 1 h at RT and then washed three times with PBST followed by addition of Nb $\alpha$ -syn01 (100 ng/mL) for 1 h at RT. In the second approach, peptides were preincubated with Nb $\alpha$ -syn01 for 2 h at RT. This was followed by the addition of the complex to a 384-well black maxisorb plate coated with full length  $\alpha$ -syn for 1 h at RT and blocked as before. In both approaches, the bound Nb $\alpha$ -syn01 was detected by addition of mouse anti-His (1/3000) antibody followed by the addition of secondary antibody (goat anti-mouse IgG-HRP). After washing, enhanced chemiluminescent substrate (Super Signal ELISA Femto, Pierce Biotechnology) was added for detection. The chemiluminescence, expressed in relative light units (RLU/s), was immediately measured using Perkin-Elmer spectrophotometer.

#### 4.7 | In-vitro $\alpha$ -syn seeded aggregation assay

In-vitro  $\alpha$ -syn seeded aggregation assay was carried out as previously described (Hmila et al., 2022). Briefly,  $\alpha$ -syn pure seeds (2  $\mu$ m) in PBS pH 7.4 were incubated alone or in combination with 10  $\mu$ m of either Nb $\alpha$ -syn01,  $\Delta$ NterNb $\alpha$ -syn01 or NbS21A in sealed 1.5 mL sterile polypropylene tubes for 1 h at 37°C with continuous shaking at 300 RPM. (total volume = 100  $\mu$ L). The incubated samples were then added to tubes containing  $\alpha$ -syn monomers in PBS to get a final concentration of 25  $\mu$ M in a total volume of 500  $\mu$ L, and the reaction mixture was further incubated at 37°C with continuous shaking at 800 RPM. Aliquots were taken out at 0, 2, 4, 6, and 24 h

intervals and immediately flash-frozen in liquid nitrogen.  $\alpha$ -Syn aggregation was determined using Th-S fluorescence assay. Each sample (10  $\mu$ L) was mixed with Th-S reagent (40  $\mu$ L–25  $\mu$ m) in PBS. Resultant fluorescence was detected in a 384-well, non-treated, black microwell plate (Nunc) with a Perkin Elmer EnVision Multimode Plate Reader using 450 and 486 nm excitation and emission wavelengths, respectively.

#### 4.8 | Accession numbers

The x-ray crystallographic data and structure coordinates were deposited in PDB (<https://www.rcsb.org/>) under accession codes: 8JLY, 8JJV.

#### AUTHOR CONTRIBUTIONS

**Zeyaul Islam:** Conceptualization; methodology; software; data curation; validation; formal analysis; visualization; writing – original draft; writing – review and editing. **Nishant N. Vaikath:** Methodology; data curation; formal analysis; validation; writing – original draft; writing – review and editing. **Issam Hmila:** Methodology; data curation; formal analysis. **Omar M. A. El-Agnaf:** Investigation; supervision; funding acquisition; writing – review and editing; project administration. **Prasanna R. Kolatkar:** Conceptualization; investigation; validation; supervision; funding acquisition; project administration; resources; writing – review and editing; visualization.

#### ACKNOWLEDGEMENTS

Crystal diffraction data were obtained using the AMX beamlines of the National Synchrotron Light Source II, a United States Department of Energy (DOE) Office of Science User Facility operated for the DOE Office of Science by Brookhaven National Laboratory under Contract No. DE-SC0012704. The Center for BioMolecular Structure (CBMS) is primarily supported by the NIH, National Institute of General Medical Sciences (NIGMS) through a Center Core P30 Grant (P30GM133893), and by the DOE Office of Biological and Environmental Research (KP1605010). We acknowledge and thank Dr Vivian Stojanoff, Dr Jean Jakoncic and Dr Alex Soares for assistance and support. We would also like to thank Mohamed Eldaw for help in shipping the crystals. Z.I., N. N. V, I.H., O.M.A.E-A, and PRK were supported by IGP3 grant from QBRI.

#### ORCID

Zeyaul Islam  <https://orcid.org/0000-0002-5444-3910>

Prasanna R. Kolatkar  <https://orcid.org/0000-0003-4970-5944>

## REFERENCES

- Adams PD, Afonine PV, Bunkóczi G, Chen VB, Davis IW, Echols N, et al. PHENIX: a comprehensive python-based system for macromolecular structure solution. *Acta Crystallogr D Biol Crystallogr*. 2010;66:213–21.
- Baba M, Nakajo S, Tu PH, Tomita T, Nakaya K, Lee VM, et al. Aggregation of alpha-synuclein in Lewy bodies of sporadic Parkinson's disease and dementia with Lewy bodies. *Am J Pathol*. 1998;152:879–84.
- Bertoncini CW, Jung Y-S, Fernandez CO, Hoyer W, Griesinger C, Jovin TM, et al. Release of long-range tertiary interactions potentiates aggregation of natively unstructured alpha-synuclein. *Proc Natl Acad Sci U S A*. 2005;102:1430–5.
- Brockhaus M, Ganz P, Huber W, Bohrmann B, Loetscher H-R, Seelig J. Thermodynamic studies on the interaction of antibodies with beta-amyloid peptide. *J Phys Chem B*. 2007;111:1238–43.
- Butler DC, Joshi SN, Genst E, Baghel AS, Dobson CM, Messer A. Bifunctional anti-non-amyloid component  $\alpha$ -synuclein nanobodies are protective in situ. *PLoS One*. 2016;11:e0165964.
- Butler YR, Liu Y, Kumbhar R, Zhao P, Gadhave K, Wang N, et al.  $\alpha$ -Synuclein fibril-specific nanobody reduces prion-like  $\alpha$ -synuclein spreading in mice. *Nat Commun*. 2022;13:4060.
- Chartier-Harlin M-C, Kachergus J, Roumier C, Mouroux V, Douay X, Lincoln S, et al. Alpha-synuclein locus duplication as a cause of familial Parkinson's disease. *Lancet*. 2004;364:1167–9.
- Chiti F, Dobson CM. Protein misfolding, functional amyloid, and human disease. *Annu Rev Biochem*. 2006;75:333–66.
- Clarke CE. Parkinson's disease. *BMJ*. 2007;335:441–5.
- Conway KA, Rochet JC, Bieganski RM, Lansbury PT. Kinetic stabilization of the alpha-synuclein protofibril by a dopamine-alpha-synuclein adduct. *Science*. 2001;294:1346–9.
- Cookson MR. The biochemistry of Parkinson's disease. *Annu Rev Biochem*. 2005;74:29–52.
- Davie CA. A review of Parkinson's disease. *Br Med Bull*. 2008;86:109–27.
- Davis IW, Leaver-Fay A, Chen VB, Block JN, Kapral GJ, Wang X, et al. MolProbity: all-atom contacts and structure validation for proteins and nucleic acids. *Nucleic Acids Res*. 2007;35:W375–83.
- de Genst EJ, Williams T, Wellens J, O'Day EM, Waudby CA, Meehan S, et al. Structure and properties of a complex of  $\alpha$ -synuclein and a single-domain camelid antibody. *J Mol Biol*. 2010;402:326–43.
- Del Mar C, Greenbaum EA, Mayne L, Englander SW, Woods VL. Structure and properties of alpha-synuclein and other amyloids determined at the amino acid level. *Proc Natl Acad Sci U S A*. 2005;102:15477–82.
- Dickson DW. Tau and synuclein and their role in neuropathology. *Brain Pathol*. 1999;9:657–61.
- Dumoulin M, Conrath K, van Meirhaeghe A, Meersman F, Heremans K, Frenken LGJ, et al. Single-domain antibody fragments with high conformational stability. *Protein Sci*. 2002;11:500–15.
- Emsley P, Cowtan K. Coot: model-building tools for molecular graphics. *Acta Crystallogr D Biol Crystallogr*. 2004;60:2126–32.
- Fares M-B, Ait-Bouziad N, Dikiy I, Mbefo MK, Jovičić A, Kiely A, et al. The novel Parkinson's disease linked mutation G51D attenuates in vitro aggregation and membrane binding of  $\alpha$ -synuclein, and enhances its secretion and nuclear localization in cells. *Hum Mol Genet*. 2014;23:4491–509.
- Forno LS. Neuropathology of Parkinson's disease. *J Neuropathol Exp Neurol*. 1996;55:259–72.
- Georgiou G, Ippolito GC, Beausang J, Busse CE, Wardemann H, Quake SR. The promise and challenge of high-throughput sequencing of the antibody repertoire. *Nat Biotechnol*. 2014;32:158–68.
- Guilliams T, El-Turk F, Buell AK, O'Day EM, Aprile FA, Esbjörner EK, et al. Nanobodies raised against monomeric  $\alpha$ -synuclein distinguish between fibrils at different maturation stages. *J Mol Biol*. 2013;425:2397–411.
- Hmila I, Vaikath NN, Majbour NK, Erskine D, Sudhakaran IP, Gupta V, et al. Novel engineered nanobodies specific for N-terminal region of alpha-synuclein recognize Lewy-body pathology and inhibit in-vitro seeded aggregation and toxicity. *FEBS J*. 2022;289:4657–73.
- Ilijina M, Hong L, Horrocks MH, Ludtmann MH, Choi ML, Hughes CD, et al. Nanobodies raised against monomeric  $\alpha$ -synuclein inhibit fibril formation and destabilize toxic oligomeric species. *BMC Biol*. 2017;15:57.
- Kabsch W. XDS. *Acta Crystallogr D Biol Crystallogr*. 2010;66:125–32.
- Krüger R, Kuhn W, Müller T, Woitalla D, Graeber M, Kösel S, et al. Ala30Pro mutation in the gene encoding alpha-synuclein in Parkinson's disease. *Nat Genet*. 1998;18:106–8.
- Li X, Duan X, Yang K, Zhang W, Zhang C, Fu L, et al. Comparative analysis of immune repertoires between Bactrian Camel's conventional and heavy-chain antibodies. *PLoS One*. 2016;11:e0161801.
- McCoy AJ, Grosse-Kunstleve RW, Adams PD, Winn MD, Storoni LC, Read RJ. Phaser crystallographic software. *J Appl Cryst*. 2007;40:658–74.
- Micsonai A, Wien F, Bulyáki É, Kun J, Moussong É, Lee Y-H, et al. BeStSel: a web server for accurate protein secondary structure prediction and fold recognition from the circular dichroism spectra. *Nucleic Acids Res*. 2018;46:W315–22.
- Mitchell LS, Colwell LJ. Comparative analysis of nanobody sequence and structure data. *Proteins*. 2018;86:697–706.
- Murshudov GN, Skubák P, Lebedev AA, Pannu NS, Steiner RA, Nicholls RA, et al. REFMAC5 for the refinement of macromolecular crystal structures. *Acta Crystallogr D Biol Crystallogr*. 2011;67:355–67.
- Muyldermans S. Nanobodies: natural single-domain antibodies. *Annu Rev Biochem*. 2013;82:775–97.
- Newell KL, Boyer P, Gomez-Tortosa E, Hobbs W, Hedley-Whyte ET, Vonsattel JP, et al. Alpha-synuclein immunoreactivity is present in axonal swellings in neuroaxonal dystrophy and acute traumatic brain injury. *J Neuropathol Exp Neurol*. 1999;58:1263–8.
- Nguyen VK, Hamers R, Wyns L, Muyldermans S. Camel heavy-chain antibodies: diverse germline V(H)H and specific mechanisms enlarge the antigen-binding repertoire. *EMBO J*. 2000;19:921–30.
- Pettersen EF, Goddard TD, Huang CC, Couch GS, Greenblatt DM, Meng EC, et al. UCSF chimera—a visualization system for exploratory research and analysis. *J Comput Chem*. 2004;25:1605–12.



- Polymeropoulos MH, Lavedan C, Leroy E, Ide SE, Dehejia A, Dutra A, et al. Mutation in the alpha-synuclein gene identified in families with Parkinson's disease. *Science*. 1997;276:2045–7.
- Qin Z, Hu D, Han S, Hong D-P, Fink AL. Role of different regions of alpha-synuclein in the assembly of fibrils. *Biochemistry*. 2007;46:13322–30.
- Reynolds NP, Adamcik J, Berryman JT, Handschin S, Zanjani AAH, Li W, et al. Competition between crystal and fibril formation in molecular mutations of amyloidogenic peptides. *Nat Commun*. 2017;8:1338.
- Rochet JC, Conway KA, Lansbury PT. Inhibition of fibrillization and accumulation of prefibrillar oligomers in mixtures of human and mouse alpha-synuclein. *Biochemistry*. 2000;39:10619–26.
- Rutherford NJ, Moore BD, Golde TE, Giasson BI. Divergent effects of the H50Q and G51D SNCA mutations on the aggregation of  $\alpha$ -synuclein. *J Neurochem*. 2014;131:859–67.
- Sircar A, Sanni KA, Shi J, Gray JJ. Analysis and modeling of the variable region of camelid single-domain antibodies. *J Immunol*. 2011;186:6357–67.
- Spillantini MG, Crowther RA, Jakes R, Cairns NJ, Lantos PL, Goedert M. Filamentous alpha-synuclein inclusions link multiple system atrophy with Parkinson's disease and dementia with Lewy bodies. *Neurosci Lett*. 1998;251:205–8.
- Staus DP, Strachan RT, Manglik A, Pani B, Kahsai AW, Kim TH, et al. Allosteric nanobodies reveal the dynamic range and diverse mechanisms of G-protein-coupled receptor activation. *Nature*. 2016;535:448–52.
- Steyaert J, Kobilka BK. Nanobody stabilization of G protein-coupled receptor conformational states. *Curr Opin Struct Biol*. 2011;21:567–72.
- Vilar M, Chou H-T, Lühns T, Maji SK, Riek-Loher D, Verel R, et al. The fold of alpha-synuclein fibrils. *Proc Natl Acad Sci U S A*. 2008;105:8637–42.
- Volles MJ, Lansbury PT. Zeroing in on the pathogenic form of alpha-synuclein and its mechanism of neurotoxicity in Parkinson's disease. *Biochemistry*. 2003;42:7871–8.
- Wakabayashi K, Yoshimoto M, Tsuji S, Takahashi H. Alpha-synuclein immunoreactivity in glial cytoplasmic inclusions in multiple system atrophy. *Neurosci Lett*. 1998;249:180–2.
- Waterhouse A, Bertoni M, Bienert S, Studer G, Tauriello G, Gumienny R, et al. SWISS-MODEL: homology modelling of protein structures and complexes. *Nucleic Acids Res*. 2018;46:W296–303.
- Wirdefeldt K, Adami H-O, Cole P, Trichopoulos D, Mandel J. Epidemiology and etiology of Parkinson's disease: a review of the evidence. *Eur J Epidemiol*. 2011;26(1):S1–S58.
- Zarranz JJ, Alegre J, Gómez-Esteban JC, Lezcano E, Ros R, Ampuero I, et al. The new mutation, E46K, of alpha-synuclein causes Parkinson and Lewy body dementia. *Ann Neurol*. 2004;55:164–73.

## SUPPORTING INFORMATION

Additional supporting information can be found online in the Supporting Information section at the end of this article.

**How to cite this article:** Islam Z, Vaikath NN, Hmila I, El-Agnaf OMA, Kolatkar PR. Structural insights into the unique recognition module between  $\alpha$ -synuclein peptide and nanobody. *Protein Science*. 2024;33(2):e4875. <https://doi.org/10.1002/pro.4875>